

Investigation of penetration forces during tufting of stacked carbon-fibre preforms

S Norouzi^{1*}, F Noerpel¹, A Matschinski¹ and K Drechsler¹

¹ Department of Aerospace and Geodesy, Technical University of Munich, Chair of Carbon Composites, Germany

*E-mail: Shima.Norouzi@tum.de

Abstract. This study investigates the penetration forces during tufting of stacked dry carbon non-crimp fabrics (NCF). The stacked material with a thickness between 20 to 60 mm is made of several quadriaxial $[0^\circ/+45^\circ/90^\circ/-45^\circ]$ NCF layers that are tufted at frequencies up to 2.3 Hz. Furthermore, the effects of the preforming process, the frequency of tufting and the thickness of specimen on the needle penetration force are investigated. Lastly, digital image correlation (DIC) is applied to study the displacement of the fabric during the unthreaded tufting of material. Future work will involve the integration of the experimental results into the simulation of the tufting process.

1. Introduction

With the dawn of the New Space era, a ten- to twenty-fold increase in the number of active spacecraft is anticipated within the next decade alone [1]. The ongoing privatization and commercialization of the spaceflight through companies such as Virgin Galactic and Blue Origin will further increase the demand on cost efficiency and reliability of spacecraft. In order to address these demands, the application of ceramic matrix composites in the rocket combustion chambers have become prominent [2]. The composite material contains a two-dimensional fibre layer construction interconnected with an additional carbon-fibre sewing thread. By means of textile technologies such as tufting, a carbon-fibre sewing thread ensures the interconnection of the stacked carbon-fibre construction. The sewing thread creates a three-dimensional shape by the alignment in the third space direction [3]. The use of thicker stacks of material and a carbon sewing thread limit the reliability of the tufting process due to failures such as needle and thread breakage.

Tufting is a one-sided sewing process without a bobbin thread that commonly applies a sinusoidal needle motion [4]. The required one-sided access to the textile favours this technology for large penetration depths. Unlike conventional sewing needles, the eye of the tufting needle is highly inclined. The bulge behind the eye of the needle pushes the thread against the surrounding textile and increases the frictional force between them. This ensures the formation and retention of the thread loops in the preform [5]. Hence, with an increasing penetration depth the friction-related penetration resistance rises. This on the other hand destabilizes the process as the needle penetration force increases. The majority of research on the measurement of forces during the sewing process is related to the garment and textile industry using common materials. The previous work on the measurement of needle penetration forces mainly focuses on the following two aspects: the development of instruments to measure the penetration forces during the sewing process [6–8] and the research on the effect of material, needle and machine properties on penetration forces, needle heating and material damage [9–11]. With regard to tufting, Sun et al. [12] simulated the penetration forces during the tufting of a 0.42 mm thick layer of non-woven fabric with a finite element analysis (FEA) model. There was an approximate agreement of the



penetration force calculated with the FEA calculation and the experimental results by other researchers [13].

There is hardly any research on the measurement of the penetration forces during tufting or sewing of carbon-fibre fabrics. The study by Verma et al. [5] is one of the few studies that determined the optimum tufting parameters for samples made of unidirectional (UD) carbon preform. Multiple layers of compacted preform layers are used for the tufting experiments. The thickness of the samples range from 2.04 mm to 20.06 mm. The penetration forces were measured at various linear tufting velocities with three different types of needle and tufting thread.

Previous research does not provide any findings to increase the reliability of the tufting process for particularly thick stacks of carbon-fibre textiles in space applications. In order to address this shortcoming, the needle penetration forces during tufting of thick stacked layers of carbon-fibre textiles must be further investigated. The present work focuses on the measurement of the penetration forces during tufting of multiple layers of non-crimp fabric (NCF) with a large total thickness (up to 60 mm). The non-threaded needle penetration experiments are performed at various sinusoidal velocities. The penetration forces are investigated for samples of various thickness at different tufting velocities. Furthermore, for a better understanding of the process, digital image correlation (DIC) is applied to measure the fabric displacement during the tufting process.

2. Experimental section

The experiments within this study are performed at two stages: 1) at loose fabric level 2) at pre-compacted preform level. The specimens made of loosely stacked layers of fabric have a fibre volume content between 35.03 % and 35.44 %, whereas the fibre volume content of the preformed specimens is 35.44 %. The force during needle insertion and retraction is evaluated for different material thicknesses at various tufting frequencies.

2.1. Materials

Carbon-fibre fabric: The material is C-PLY™ SP Q220/P23 CT3,4 12K HS from Chomarat that is a quadriaxial NCF with the total weight of 220 gsm, i.e. 55 gsm/ply. The NCF is made of 12 K-strength carbon fibres and the UD fibres are oriented at $0^\circ/+45^\circ/90^\circ/-45^\circ$. The material contains a binder that is powdered on one side between the layers of UD fibres.

Tufting needle: The needle has a quadratic cross-section and is exclusively designed for the tufting process. It is a KL150 GEBEDUR with a length of 90 mm from Groz-Beckert KG.

2.2. Sample preparation

The specimens for penetration tests consist of multiple layers of 100 mm x 100 mm material stacked on top of each other, with the -45° side of the material facing upwards. The specimens are of three different thicknesses: 20 mm, 40 mm and 60 mm. The preforming process requires binder activation. For the pre-compacted specimen, the loosely stacked layers of fabric are heated up to 120 C while being compressed to a predefined height. The required height is ensured by placing aluminium spacers on each side of the specimen during the compression process. The penetration tests are conducted on specimens at room temperature.

2.3. Testing equipment and setting

A ZwickRoell HC25 servo-hydraulic universal testing machine provides the test set-up for the penetration experiments. For the purpose of this study, a 2 kN load cell is used. Similar to the real sewing process, the motion of the needle during the experiments follows a single cycle of a cosine function (sinusoidal velocities instead of linear). The amplitude and frequency of the cosine function are variable and are chosen based on the thickness of the stacked material and the required tufting velocity.

Aluminium profiles ensure the mount on the test jig of the servo-hydraulic machine (see Figure 1). A 3 mm gap between the two topmost aluminium profiles is aligned with the needle insertion path. This prevents the tufting needle from contacting the aluminium structure upon piercing through the entire thickness of the specimen. Four nuts compact the specimen to ensure a level surface for needle insertion by an aluminium plate. An aluminium plate with a centred hole (40 mm diameter) compresses the

stacked layers of material into a predefined height using aluminium spacers. Four nuts hold and press the aluminium plate down and ensure a level surface for needle insertion.

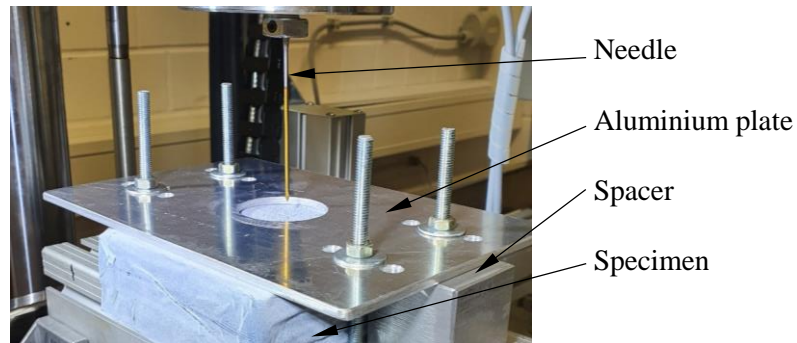


Figure 1. Set-up for the needle penetration experiments.

Due to performance limitation, the maximum frequency of 1 Hz is chosen for the tests on the thickest specimens (60 mm). To investigate the effect of different frequencies on the penetration force, the 60 mm specimens are tested at 0.5 Hz, 0.7 Hz and 1 Hz frequencies. The amplitude of the cosine function is chosen to be 5 mm larger than half of the specimen's thickness. This way the needle's motion starts above the specimen's surface and needle retraction occurs once the tip of the needle has entirely exited the other side of the specimen.

In order to achieve comparable results for different thicknesses, the properties of the cosine function describing the motion of the needle in time need to be adjusted. The following equation is used to determine the frequencies for the 20 mm and 40 mm specimens: $F_i \cdot A_i = F_j \cdot A_j$. Thus, for different specimen thicknesses, the maximum needle insertion velocity remains constant. Table 1 shows the properties applied to create the needle time-path function for respective specimen thicknesses.

Table 1. Properties of the time-path cosine function for respective specimen thickness.

Thickness (mm)	Amplitude (mm)	Frequency F_1 (Hz)	Frequency F_2 (Hz)	Frequency F_3 (Hz)
60	35	1	0.7	0.5
40	25	1.4	0.98	0.7
20	15	2.33	1.63	1.17

In order to measure the displacement of the material's surface during penetration testing, a dual camera ARAMIS System is used. The cameras are Teledyne DALSA PT-4104M60 with a resolution up to 2352 x 1728 pixels and a maximum frame rate of 60 Hz. The applied lenses have a focal length of 100 mm. To measure the displacement, a random black-on-white speckle pattern has to be applied to the specimen's surface. The cameras track the movement of the speckle pattern and the displacement of the surface can be calculated based on the DIC measurement technique.

3. Results and Discussion

The needle penetration force is measured during a single needle insertion and retraction into and from the specimens. Figure 2 shows the force-path diagram of a single tuft into a 60 mm loosely stacked specimen at 0.5 Hz frequency. The diagram maps the force acting upon needle to the position of the needle. The penetration of the needle into the specimen causes a counterforce that acts upon the needle. This appears as a negative force in the force-path diagram in Figure 2. The needle path starts at the upper dead point. For 60 mm thickness, the upper dead point of the cosine motion is at +35 mm, which corresponds to a path position at 0 mm. At this point, the force is equal to 0 kN. The lower dead point of the cosine function is set to -35 mm that is equal to a path = 70 mm and a force = 0 kN. The retraction of the needle from the material causes a tensile force. This tensile force appears as a positive force on the needle in the force-path diagram in Figure 2.

The force–path diagram can be divided into six areas. Area a indicates the 5 mm distance of the needle tip from the specimen’s surface. In this area, the needle motion has started, however, the needle tip has not made contact with the specimen’s surface. Area b marks the start of the needle tip penetration into the material. Within this area, the bulge of the needle begins to compress the surrounding textile prior to its penetration into the specimen. The force–path diagram in this area is the result of the reaction force of the material as the needle tip pierces through it. In area c, the bulge of the needle begins to pierce through the material. The approximately constant increase in the force is the result of the hole formation and the growing friction between the needle and carbon fibres as the needle taper further penetrates the material. With the growing friction, the sliding between the needle and the carbon fibres onsets. This evokes the so-called stick-slip effect that results in a fluctuating penetration force (see the jagged curve within area d). In area e, the needle tip pierces the last layers of fabric. There are less underlying layers of fabric that resist the compressive force of the needle bulge. Hence, the compressive force is able to cause a greater deflection of the underlying layers. The penetration force decreases approximately constantly until the needle’s bulge leaves the material. Area f marks the exit of the bulge from the bottom side of the specimen. In this area, the frictional force between the carbon fibres and the needle is the dominant force. Needle retraction from the specimen onsets once the lower amplitude of the cosine function is reached. Needle retraction takes place through the same trajectory as the needle insertion. Hence, no hole formation is required. The positive force indicates the tensile force on the needle during the retraction from the specimen. This force is mainly the result of the frictional force between the carbon fibres and the needle. This depends on the area of the needle that is still inside the specimen. The force decreases in a constant manner until the needle completely exits the material.

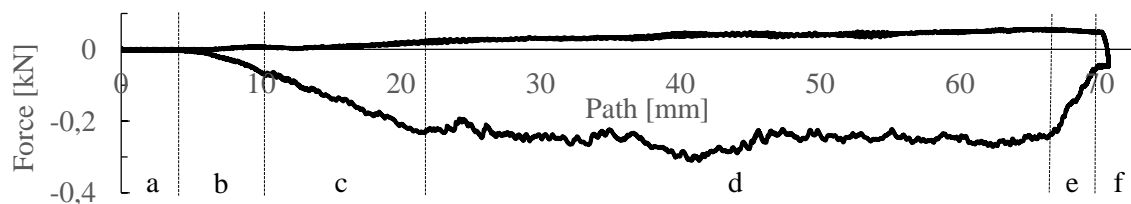


Figure 2. Force–path diagram of a 60 mm loosely stacked specimen tested at 0.5 Hz

Influence of the pre-compaction process on the penetration force: Figure 3 shows the force–path diagrams related to a loosely stacked and a pre-compacted specimen (40 mm thickness, at 0.7 Hz tufting frequency). The dotted line indicates the loosely stacked specimen, whereas the solid line belongs to the pre-compacted specimen. For both specimens, needle insertion initially results in an approximately constant increase in the force. For the pre-compacted specimen, the force due to the needle insertion increases more rapidly as the associated slope of the curve is higher. The course of the jagged area for both specimens is somewhat similar. However, for the pre-compacted specimen, the absolute value of force within this area is larger than that of the loosely stacked specimen. The pre-compacted fibres exhibit a higher resistance towards the penetration of the needle. For the pre-compacted specimen, the fluctuating force within this area shows larger peaks. The connection between the fibres becomes stiffer due to binder activation. Hence, the bending stiffness of the fabric increases on macroscopic scale. During hole formation, the fibres are more prone to getting caught at the needle’s surface and impede the motion of the needle. This causes a small peak in the penetration force. As the needle further penetrates the material, the stuck fibres bounce back and the peak in the force declines. This phenomenon leads to the jagged form of the curve within this area. The stiffer structure within the pre-compacted specimen leads to more dominant peaks in the force–path diagram. The comparison of the needle retraction curves makes evident, that the frictional force between the carbon fibres and the needle’s surface is higher for the pre-compacted specimen.

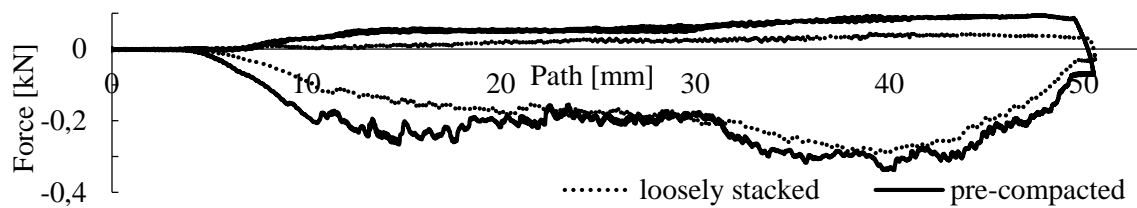


Figure 3. Force-path diagram of 40 mm specimens tested at 0.7 Hz tufting frequency.

Influence of the tufting frequency on the penetration force: In order to investigate the effect of the tufting velocity, a loosely stacked specimen tested at three different frequencies is considered (Figure 4). The specimen with a total thickness of 60 mm is tested at frequencies of 0.5 Hz, 0.7 Hz and 1 Hz. As Figure 4 shows, the force-path curves for all three frequencies are very similar. The slight differences are related to the scatter of force that even occurs for two identical experiments. Hence, an identical penetration experiments do not result in identical force-path diagrams. For identical experiments, the local imperfections in the fibre orientation within the layers lead to small deviations in the force. The subtle differences between the curves suggest that the tufting velocity does not have a prominent influence on the penetration force. Pre-compacted specimens tested at various frequencies show a similar behaviour.

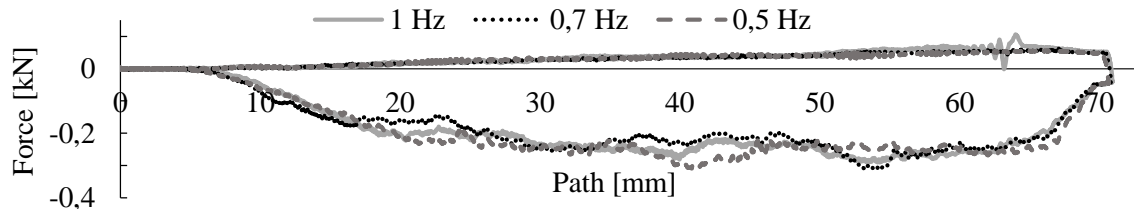


Figure 4. Force-path diagram of a 60 mm loosely stacked specimen at various tufting frequencies.

Influence of the specimen's thickness on the penetration force: In order to evaluate the influence of the specimen's thickness on the force, three different thicknesses are compared. Figure 5 demonstrates three loosely stacked specimens tested at their minimum frequency. The frequencies are chosen based on the thickness of the specimen (see Table 1). Figure 5 shows that a smaller thickness results in a smaller path in the force-path diagram. Regardless of the specimen's thickness, all three needle insertion curves show an initial constant increase with a similar slope. At about 20 mm path position, the insertion curve related to the 20 mm specimen starts to decline until needle retraction onsets. At this point, the compressive force on the needle reaches a maximum of -0.19 kN. The curve related to the 40 mm specimen continues to rise with a smaller slope. The compressive force on the needle reaches a maximum of -0.29 kN at about 40 mm path position before the curve starts to decline. The 60 mm specimen shows a similar behaviour. After an initial constant increase in the force, the curve increases with a smaller slope. The maximum compressive force for this specimen is not significantly larger compared to the 40 mm specimen. The maximum compressive force occurs at about 42 path position and is equal to -0.31 kN. The needle retraction curves of all three specimens have a constantly decreasing behaviour with similar slopes.

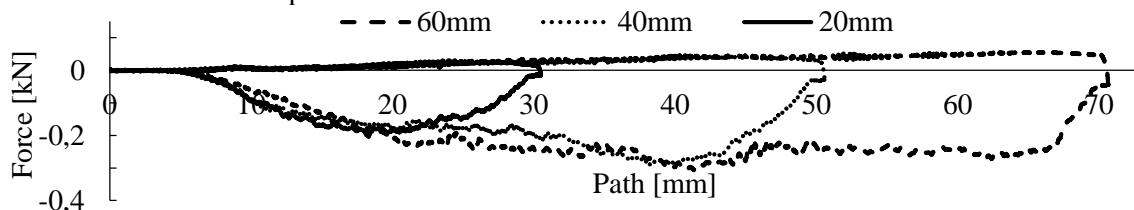


Figure 5. Loosely stacked specimens of various thickness tested at their minimum frequency.

Displacement of the material during needle penetration: Displacement at the surface of the specimen is measured by the means of ARAMIS system. The rapid motion of the needle and the strong vibration of material result in blurred images at the moment of impact and shortly after. Therefore, these images,

captured at 60 Hz frame rate, cannot be evaluated. Furthermore, shortly before the arrival of needle at the bottom dead point the camera views are obscured by the jaw chuck of the servo-hydraulic machine. Therefore, the measurement of the material's displacement do not result in a continuous curve. Despite this limitation, the displacement of the specimen's surface in z-direction can be measured. Figure 6 and Figure 7 show the z-direction displacement of a point nearby the needle insertion for a pre-compacted 60 mm specimen at 0.5 Hz and 1 Hz tufting frequencies. Negative values of displacement are related to needle insertion whereas the positive values are due to needle retraction from the specimen. Both diagrams consist of multiple individual curves, interrupted by areas for which no evaluable images are captured. Both diagrams suggest that the maximal absolute value of displacement occurs at the beginning of needle insertion. This value cannot be measured as the moment of the needle insertion and shortly after cannot be evaluated. However, the maximal measured displacement due to needle insertion is -1.88 mm at 1 Hz tufting frequency (Figure 6). For 0.5 Hz tufting frequency, the maximum measured displacement is equal to -2.99 mm (Figure 7). Moreover, the diagrams demonstrate that needle retraction induces an outwards displacement in the surface of the specimen. This does not return to its original position even after needle retraction is completed. The remaining displacement for the experiment at 1 Hz is +0.33 mm, whereas at 0.5 Hz a residual displacement of 0.7 mm is measured. The diagrams imply that at a lower frequency a larger displacement in z-direction occurs. As the frequency decreases, the relative motion between the needle and the surrounding material decreases. Thus, the static friction effects outweigh the sliding friction effects. The frictional effects predominate the inertia of the masses of the surrounding material. This leads to a larger displacement of the surrounding material with decreasing tufting frequency. This behaviour is reversed for an increasing tufting frequency.

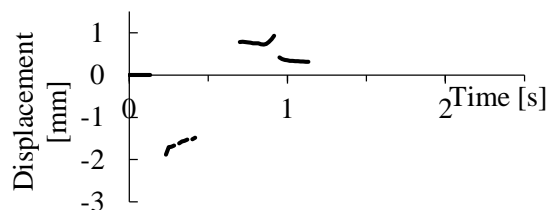


Figure 6. Displacement in z-direction during penetration testing of a 60 mm specimen at 1 Hz.

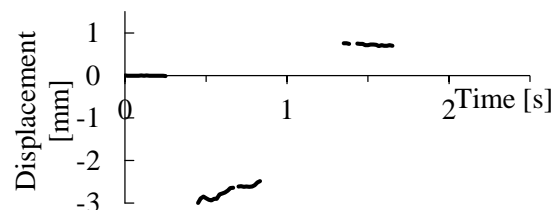


Figure 7. Displacement in z-direction during penetration testing of a 60 mm specimen at 0.5 Hz.

4. Conclusions and outlook

This study investigated the penetration forces on the needle during unthreaded tufting of stacked layers of NCF with a total thickness up to 60 mm. The influence of the preforming process, the thickness of specimen and the tufting frequency on the penetration force were analyzed. The displacement of material in z-direction due to needle insertion and retraction was measured. The following conclusions can be drawn from this study:

- The pre-compaction process leads to an increased needle penetration force within the tufting process as the activated binder and the stiffer material structure impede the motion of the needle within the specimen. The maximum force is higher for both needle insertion and retraction process.
- The needle penetration force is not dependent on the tufting velocity, i.e. regardless of the frequency of tufting similar penetration forces were measured under otherwise same conditions.
- A higher specimen's thickness leads to a higher maximum penetration force as the needle travels a larger path in order to pierce through the material. This holds true for both needle insertion and retraction. However, the initial increase in the insertion force for specimens of all thicknesses occurs at the same slope. The slope of the needle retraction curves remains the same regardless of the specimen's thickness.
- A smaller tufting velocity results in a larger displacement in z-direction in an area nearby the needle insertion point.

The results of this study indicate the complex nature of the resistance forces that appear during tufting. A detailed investigation requires the simulation of the penetration forces. Future work will focus on creating a simulation model for a detailed study of penetration forces during tufting of particularly thick stacks of carbon fibre fabrics.

5. Acknowledgements

The authors thankfully acknowledge the funding at TUM provided by the German Federal Ministry for Economic Affairs and Energy under the scheme “ZIM: Zentrales Innovationsprogramm Mittelstand” (funding code: ZF4004320PO9). Great appreciation is expressed to Groz-Beckert KG for providing the tufting needles for the conduction of the experiments within this study. Finally, the authors would like to thank Ariane Group and SGL Carbon SE for the valuable knowledge transfer.

References

- [1] Oltrogge D and Christensen I 2020 Space governance in the new space era *J. of Space Safety Eng.* **7** 432–8
- [2] Ortelt M, Seiler H, Boehleb M and Munkc D 2019 *Black Engine Ceramic Rocket Propulsion* 70th Int. Astronautical Congress IAC, Washington DC
- [3] Beyer S, Knabe H and Preklik D 2005 *Combustion Chamber with Internal Jacket Made of a Ceramic Composite Material and Process for Manufacture* United States Patent (US006890660B2)
- [4] Mallet E and Du R 1999 Finite element analysis of sewing process *Int. J. of Clothing Sci. & Technol.* **11** 19–36
- [5] Verma K, Padmakara G, Gaddikeri K, Ramesh S, Kumar S and Bose S 2019 *Composites Part B: Engineering* **174** 106970
- [6] Carvalho H, Monteiro J and Ferreira F 1997 *Measurements and Feature Extraction in High-Speed Sewing* 97th Proc. of the IEEE Int. Symp. on Industrial Electronics Guimaraes, Portugal, 7-11
- [7] Carvalho H, Rocha A and Monteiro J 2009 Measurement and Analysis of Needle Penetration Forces in Industrial High-Speed Sewing Machine *J. of the Textile Institute* **100** 319–29
- [8] Matthews BA and Little T 1988 Sewing Dynamics *Textile Research J.* **58** 383–91
- [9] Khan R, Hersh S and Grady P 1970 Simulation of Needle-Fabric Interactions in Sewing Operations. *Textile Research J.* **40** 489–98
- [10] Stylios G. 1987 *A Study of Problems Associated with Fabric Sewing in Commercial Garment Manufacture* (PhD thesis, University of Leeds)
- [11] Hearle J and Sultan M 1968 A study of needled fabrics Part VI: The measurement of Punching *J. of the Textile Inst.* **59** 237–42
- [12] Sun Y, Gao X, Meng Z, Xu Y and Ma X 2013 Finite element analysis of penetration force for needle during tufting process *J. of the Textile Inst.* **104** 745–54
- [13] Shaoping Z and Caihong D 2008 Force measurement of needle bar in process of carpet tufting and related process analysis *Textile Research J.* **29** 108–11